Periodica Polytechnica Mechanical Engineering

Mechanical Behavior of Layered Composite Structures of Aluminum Foam Partially Filled with Polyamide

Wanrong Du[1*], Imre Norbert Orbulov[1,2], Péter Tamás-Bényei[3,4,5], Csilla Kádár[1,2]

[1] Department of Materials Science and Engineering, Faculty of Mechanical Engineering, Budapest University of Technology and Economics, Műegyetem rkp. 3., H-1111 Budapest, Hungary
[2] MTA–BME Lendület "Momentum" High-performance Composite Metal Foams Research Group, Műegyetem rakpart 3., H-1111 Budapest, Hungary
[3] Department of Polymer Engineering, Faculty of Mechanical Engineering, Budapest University of Technology and Economics, Műegyetem rkp. 3., H-1111 Budapest, Hungary
[4] HUN-REN-BME Research Group for Composite Science and Technology, Műegyetem rkp. 3, H-1111 Budapest, Hungary
[5] MTA-BME Lendület Sustainable Polymers Research Group, Műegyetem rkp. 3, H-1111 Budapest, Hungary
* Corresponding author, e-mail: duwanrong@edu.bme.hu

Abstract

In this study, the mechanical properties of layered composite structures were investigated. We achieved the layered structure by hot-pressing 1 mm, 3 mm, or 5 mm thick polyamide 6 (PA) sheets into the pores on the top and bottom sides of an open-cell metal foam at 240 °C and 15 MPa (150 bar). The PA-infiltrated depths varied with the thickness of the hot-pressed PA sheets. According to the bending and post-impact bending tests, flexural strengths improved as the infiltration depth of PA increased. Compared to the metal foam, a maximum of 15% increase in flexural strength and a 400% increase in residual flexural strength were measured. However, using a 1 mm thick PA sheet lowered the flexural strength of the open-cell metal foam. We found that the 1 mm thick PA sheet failed to fully infiltrate the foam pores, resulting in residual voids at the metal-PA interface, which caused premature fracture during bending.

Keywords

metal foam, composite, three-point bending test, post-impact residual strength

1 Introduction

The application of lightweight materials in the transportation industry has become widespread in recent years due to their ability to reduce weight, which has improved fuel efficiency and reduced environmental impact [1, 2]. Thus, the development of new lightweight materials with higher specific strength and stiffness has become very important.

Automotive body structures may experience multiple impacts throughout their service life, so understanding their post-impact residual strength is critical. Many studies have focused on compression after impact testing [3–5] to evaluate the residual strength of impact sandwich panels. However, sandwich panels in automobile bodies are typically required to resist bending loads, and therefore, it is necessary to test their bending behavior after impact.

Metal foams are a new class of material, made by a range of novel manufacturing techniques. They have a high strength-to-weight ratio and good energy absorption capacity, thus, they are often used in the design of lightweight

materials [6, 7]. Due to their cellular structure, they are filled into hollow sections or used as a core material in sandwich panels to enhance resistance to bending load [8–10].

Omar et al. [8] studied a metal matrix syntactic foam (MMSF) core sandwich panel composed of alumina hollow particles reinforced A356 alloy syntactic foam and carbon fabric skin, and characterized its performance under three-point bending conditions. The test results showed that the average flexural strain of the MMSF core sandwich composite was 0.49 ± 0.06% and the stiffness was 20.6 ± 0.7 GPa. Kemény et al. [9] investigated the compressive and flexural strength of MMSF filled into various empty hollow sections. They found that an epoxy-bonded foam-filled hollow section structure (adhesive thickness 1.0 mm, density 1.13 g/cm³, overlap shear strength 38 MPa at 24 °C) showed a 12% and 25% increase in energy absorption in square and rectangular geometries, respectively, compared to the sum of the energy absorption of the foam

and empty hollow section. Huang et al. [10] investigated the metallurgical-bonding interface-formation mechanism of aluminum foam sandwich (AFS) prepared by powder metallurgy and analyzed the bending performance and energy absorption of metallurgical bonding AFS and glued AFS. The results showed that the peak load of metallurgically bonded AFS was 24% higher than that of glued AFS, and the energy absorption was 12.2 times that of glued AFS.

The manufacturing process determines the mechanical properties of sandwich panels, especially under bending and impact loads, which has an important effect on the flexural strength, energy absorption characteristics, and failure mechanism [11–16]. The performance of a sandwich panel depends heavily on the quality of the bond between the face sheets and the core material. Delamination can happen if the interface layer is improper, which can decrease the mechanical properties and the stability of the sandwich panel [17–19].

Our goal was to produce a lightweight structure with enhanced flexural strength and post-impact bending properties. For that, we designed a new type of layered composite with three layers, where the upper and lower layers were metal-polyamide 6 (PA) composites, while the middle layer was metal foam. To avoid delamination during bending, the layered structure was made out of a single block of metal foam. The layered structure was achieved by hot-pressing PA into the pores in the top and bottom layers of the open-cell foam. The effect of PA content on the bending and post-impact properties was investigated.

2 Materials and methods
2.1 Sample preparation
PA granules and Al - 12 wt% Si (AlSi12) open-cell metal foams were selected to produce composites with layered structure. The chemical composition of the metal foam material is given in Table 1.

The open-cell metal foam was manufactured by the salt replication method. First, salt particles with 3–4 mm size were sintered at 800 °C for 2 h to form an interconnected

Table 1 Chemical composition of the metal material (AlSi12)

Element	Composition (wt%)
Al	bal.
Si	12.5
Fe	0.542
Mn	0.152
Ti	0.140
Other	0.037

structure. Subsequently, the AlSi12 was heated in an induction furnace (Lindberg Blue M), and the sintered salt, preheated to 400 °C, was infiltrated by the molten AlSi12 using argon gas at 450 kPa (4.5 bar). After the metal was cooled down to room temperature, the foam blocks were cut into 20 mm thick slices. Finally, the salt was leached out by running water, resulting in an open-cell metal foam with a pore size of 3–4 mm.

From these AlSi12 foam slices, metal foam-PA composites were produced using the hot-pressing method. First, PA granules (A. Schulman, Inc., USA) were dried in a drying oven (Venticell LSIS-B2V) at 80 °C for 24 hours to remove moisture. Then, the granules were hot-pressed in a hot-pressing machine (Teach-Line Platen Press 200E) at 235 °C for 5 minutes and cooled for 10 minutes to form PA sheets with thicknesses of 1 mm, 3 mm, and 5 mm. The prepared PA sheets were hot-pressed into the top and bottom of the AlSi12 metal foam at 240 °C and 15 MPa (150 bar) pressure to create the layered composites. The metal foam-PA composites are referred to as PA_1, PA_3, and PA_5, where the number indicates the thickness of the PA layers that were hot-pressed into the AlSi12 foam's pores. With this procedure, the middle layer remained metal foam. With each parameter set, two 74 mm × 74 mm × 20 mm panels were produced. Fig. 1 shows the schematic diagram of the fabrication process.

2.2 Material characterization
For each type of metal foam-PA composite, 12 images made by a stereomicroscope (Olympus SZX16) were used for the structural analysis. The depth of the hot-pressed PA in the metal foam (infiltration depth) was measured on cross-sections of the samples in 30 points using ImageJ image processing software [20]. The fracture surface after the bending test was investigated with a scanning electron microscope (ZEISS EVO MA 10).

A Zwick Z020 tester machine was used to carry out the three-point bending test at room temperature with a cross-head speed of 5 mm/min. The loading head and the supports were steel cylinders with a diameter of 10 mm and a span of 40 mm. The bending tests of the samples
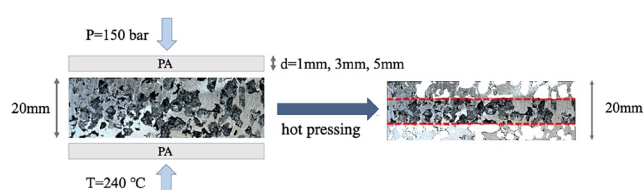

Fig. 1 The schematic diagram of the manufacturing process

were video recorded. The size of the rectangular samples was 74 mm × 20 mm × 20 mm. For each type of material, 3 samples were tested. The flexural strength (σ_f) was calculated from the maximum load (F_m), according to Eq. (1),

$$\sigma_f = \frac{3F_m L}{2bh^2},\qquad(1)$$

where L is the support span and b and h are the width and thickness of the specimen, respectively.

The Charpy impact test was conducted using a Ceast Resil Impactor Junior tester. The blocks' size of unnotched specimens for Charpy impact tests and post-impact residual strength tests were 74 mm × 10 mm × 20 mm. The impact damage threshold (critical energy) for the residual strength was set as 1 J based on the nearly invisible damage (BVID) method [21]. The Charpy impact strength was calculated according to the MSZ EN ISO 7438:2021 standard [22]. In the post-impact residual strength test, the surface experiencing a 1 J impact was placed flatwise. For the impact and post-impact test, 3-3 samples were tested.

The density of each sample was calculated as the ratio of mass to volume. The volume was calculated as the product of the length, width and thickness of the sample measured with a caliper.

3 Results and discussion
3.1 Microstructure
Fig. 2 shows the cross-sections of the layered composites. The resulting structure can be divided into three layers: the upper and lower layers are PA-metal composites, while the middle layer remains AlSi12 foam, similar to sandwich structures.
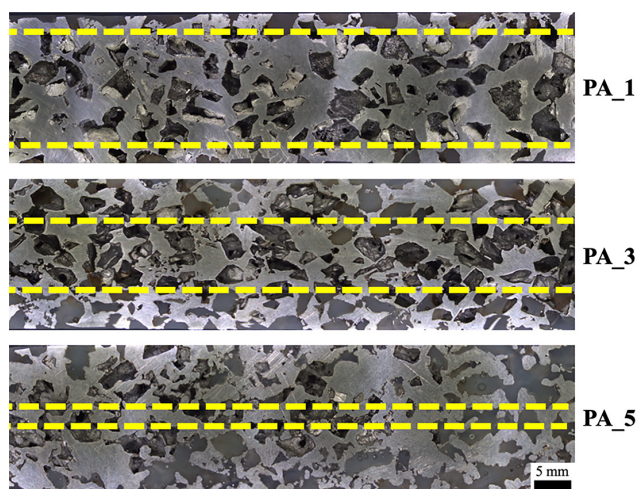

PA_1

PA_3

PA_5

5 mm

Fig. 2 The structure of the layered composites (The yellow dash lines indicate the layers of the composites.)

Table 2 presents the structural parameters of the samples: the metal area fraction (S_{metal}/S), PA area fraction (S_{PA}/S), and pore area fraction (S_{pores}/S) that were determined on the cross-sectional surfaces of the samples. The Depth_top and Depth_bottom indicate the infiltration depth of PA in the AlSi12 metal foam, measured on the cross-sectional surface from the top and bottom, respectively.

The infiltration depth increases with PA content, indicating that the chosen hot-pressing parameters result in a good manufacturing process. The infiltration depth is less than the pore size of the AlSi12 foam for PA_1 samples, indicating that only the pores on the surface are filled with PA. In the case of PA_5, the infiltration depth is about twice the pore size. As the infiltration depth depends on the interconnectivity of the pores, the higher the infiltration depth, the higher the scatter is.

During the hot-pressing process, the infiltration of the bottom PA sheet into the metal foam was less successful as part of the molten PA flow out in the lateral direction, while the top PA sheet infiltrated deeper, resulting in the asymmetrical infiltration of the PA on the top and bottom sides of the metal foam- PA composite.

When the thickness of the PA sheet used increases, S_{PA}/S increases and S_{pores}/S decreases, and thus, the density of metal foam-PA composite increases. The infiltration depth of PA also increases on both the top and bottom sides of the foam.

To investigate the metal-PA interface, the fracture surface of the foam-PA samples was investigated. The SEM images of fracture surfaces after three-point bending tests are shown in Fig. 3. The red and blue arrows indicate the AlSi12 metal foam and the PA, respectively, and the green dashed line shows the metal-PA interface.

Fig. 3 (a) shows that in the case of PA_1, the infiltration of the foam's pores was not complete, as there are some

Table 2 Structural parameters of the samples; S_x/S denotes the area fraction of material X, and Depth is the infiltration depth of PA in the metal foam from the top and the bottom

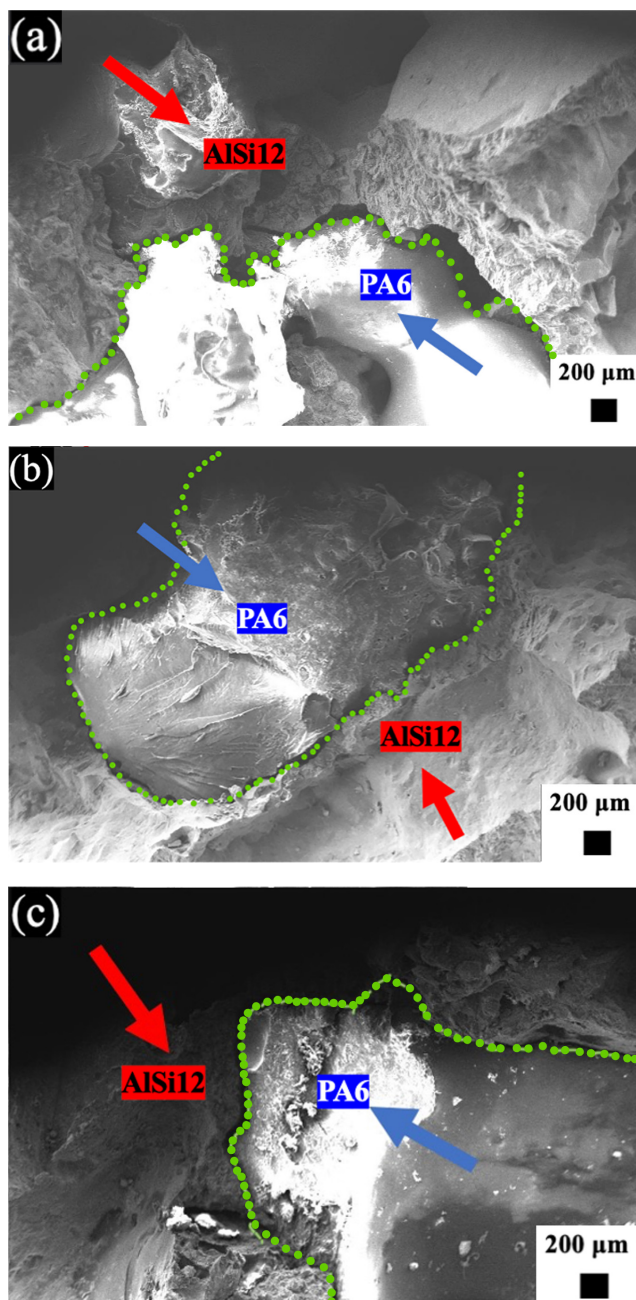|	AlSi12 foam	PA_1	PA_3	PA_5
S_{metal}/S (%)	47.2 ± 2.5	49.6 ± 1.8	47.6 ± 5.0	44.5 ± 2.8
S_{PA}/S (%)	-	9.4 ± 1.0	18.3 ± 1.8	41.4 ± 2.4
S_{pores}/S (%)	52.8 ± 2.5	41.0 ± 2.8	34.1 ± 5.5	14.1 ± 4.5
Depth_top (mm)	-	2.1 ± 0.6	4.6 ± 0.9	9.8 ± 1.4
Depth_bottom (mm)	-	1.6 ± 0.1	4.0 ± 1.1	8.2 ± 2.0
Density (g/cm³)	1.21 ± 0.05	1.25 ± 0.05	1.44 ± 0.01	1.54 ± 0.03

Fig. 3 Metal-PA interface in metal foam-PA composite with different PA content: PA_1 (a), PA_3 (b), PA_5 (c)

remnant voids between the metal and PA. As the PA content is increased, the infiltration of the pores is better, indicating that the manufacturing process results in a better infiltration process with increasing PA content. However, in many cases, the metal and the PA surfaces are partly separated (Fig. 3 (b), (c)).

3.2 Three-point bending test

The effect of PA content on the AlSi12 metal foam's mechanical properties was studied. Fig. 4 shows the three-point bending curves and Table 3 displays the flexural
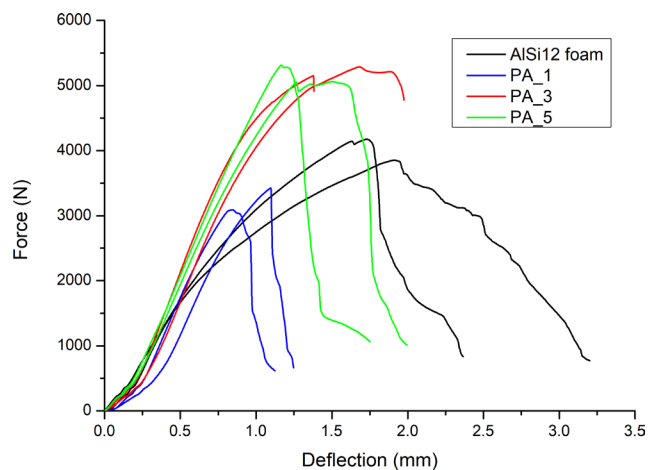

Fig. 4 The load-deflection curves for AlSi12 foam (black), PA_1 (blue), PA_3 (red) and PA_5 (green)

Table 3 The flexural strength (σ_f), the specific flexural strength (σ_f/ρ), residual strength ($\sigma_{f,res}$) and specific residual strength ($\sigma_{f,res}/\rho$) of metal foam-PA composites without and after impact

Sample	σ_f (MPa)	σ_f/ρ (MPa·cm³/g)
AlSi12_foam	33.7 ± 2.6	24.8 ± 1.7
PA_1	26.8 ± 2.8	23.0 ± 2.2
PA_3	36.0 ± 1.7	26.8 ± 1.5
PA_5	39.0 ± 3.0	26.3 ± 2.8
Sample	$\sigma_{f,res}$ after 1 J Impact (MPa)	$\sigma_{f,res}/\rho$ after 1 J Impact (MPa·cm³/g)
AlSi12_foam	9.2 ± 5.1	8.5 ± 4.6
PA_1	24.7 ± 5.4	18.4 ± 3.4
PA_3	48.5 ± 2.6	31.6 ± 1.6
PA_5	47.4 ± 11.4	29.9 ± 7.0

strength, specific flexural strength, residual strength and specific residual strength of AlSi12 foam and the composites with different PA content. For better visibility, only two load-deflection curves from each type of sample are shown in Fig. 4 to reflect the bending behavior.

The PA_1 samples have the lowest flexural strength, even lower than the flexural strength of the AlSi12 foam. This phenomenon shows that in this case, the PA fails to strengthen the AlSi12 foam. As the microstructural investigation revealed, in the case of PA_1 only the pores on the surface were filled with PA resulting in a highly uneven reinforcement thickness, and in many cases remnant pores at the metal-PA interface were found. During bending test, these may lead to stress concentration, thereby triggering rapid failure [23–25]. According to Table 3, the flexural strength increases with increasing PA content, and PA_5 has the highest flexural strength. However, the difference in flexural strength for PA_3 and PA_5 is not significant, indicating that from the point of view of flexural strength,

PA_3 may be the best choice, especially so as the specific flexural strength (flexural strength to density ratio) is the highest for PA_3. However, as Fig. 4 shows the load-deflection curves of PA_3 (red curves) stop almost right after the maximum stress, which is due to the sudden drop in force.

Fig. 5 shows the macro failure mechanisms of foam and foam-PA under the three-point bending condition. After reaching the maximum stress, the curve starts to decrease; for foam samples the force decreases gradually, for PA_1 and PA_5 rapidly, and for PA_3, there is a sudden drop in force. The video recording showed that the direction of crack propagation in the foam samples was not vertical (i.e. in the direction of the load), causing the gradual decrease in force. In the case of foam-PA samples, the crack propagation was vertical, and for PA_3 the crack already propagated through the sample when reaching the maximum force, causing the abrupt force drop. In the case of PA_5, the upper metal-PA layer hindered somewhat the crack propagation, resulting in a rapid force decrease.

3.3 Charpy impact test

Table 4 presents the Charpy impact strength and specific Charpy impact strength (Charpy impact strength to density ratio) of the foam and foam-PA samples.

The Charpy impact test results show that the foam-PA sample's ability to resist local impact increases with increasing PA content. As the PA content in the foam increases, the impact strength of the foam-PA sample also increases. Similarly to flexural strength, the Charpy impact strength of PA_3 and PA_5 is almost the same, which may be due to the similar failure mechanism as for bending. The Charpy impact strength of AlSi12 metal
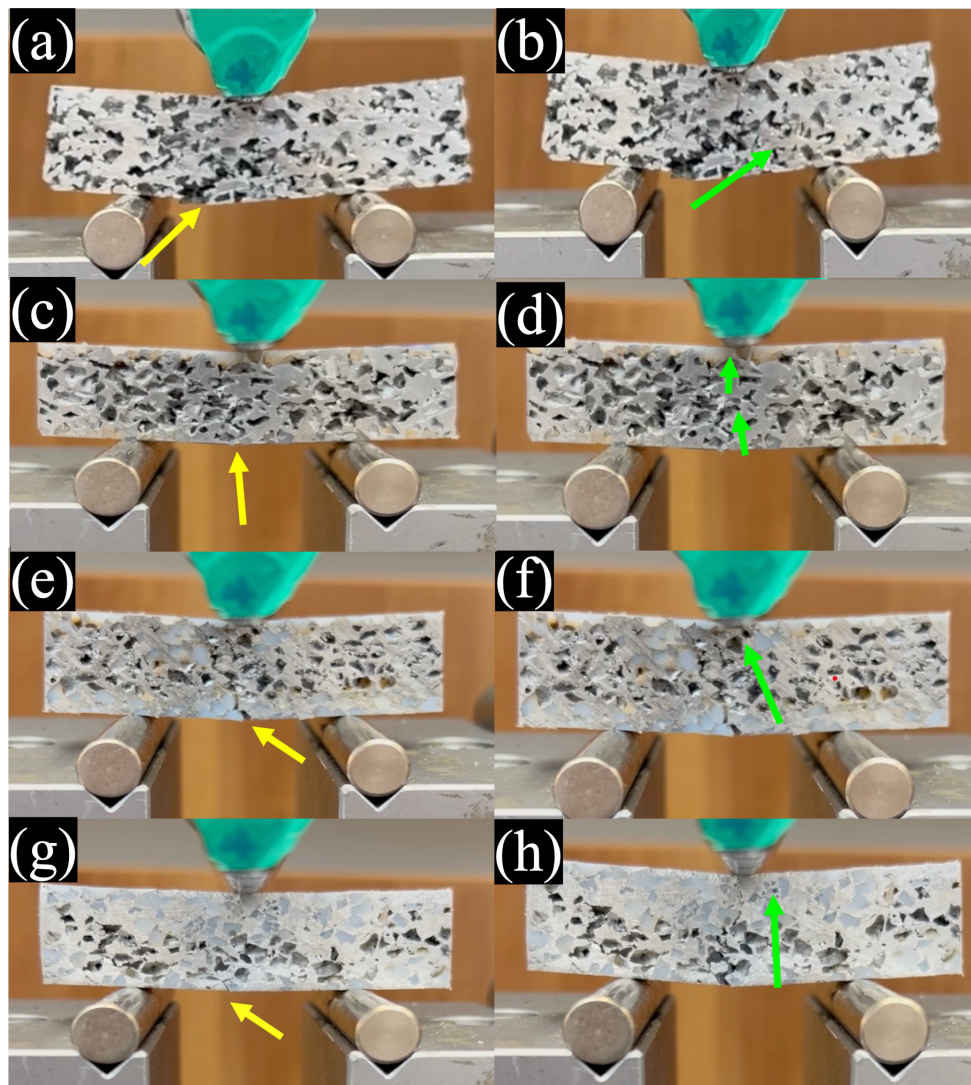

Fig. 5 The bending behavior of foam at maximum load (a), foam after removing the load (b), PA_1 at maximum load (c), PA_1 after removing the load (d), PA_3 at maximum load (e), PA_3 after removing the load (f), PA_5 at maximum load (g) and PA_5 after removing the load (h) (The yellow and green arrows show the place of crack initiation and the direction of crack propagation, respectively.)

Table 4 Charpy impact strength and specific impact strength of AlSi12 foams and AlSi12 foam samples with different PA content

Sample	Average Charpy impact strength (kJ/m^2)	Average specific Charpy impact strength (σ_i/ρ) (kJ/m^2) / (g/cm^3)
AlSi12 foam	77.8 ± 2.0	65.1 ± 2.4
PA_1	24.3 ± 3.9	18.4 ± 2.7
PA_3	40.3 ± 8.5	28.0 ± 3.9
PA_5	50.8 ± 10.3	31.2 ± 6.3

foam is the highest, almost 1.5 times higher than that of PA_5. As the bending tests showed, adding PA increases the maximum force the samples can withstand, and thus, it results in an increase in flexural strength. However, the absorbed energy during bending is the highest in the case of the foam sample, as the addition of PA causes a drop in force after the peak stress, reducing the absorbed energy during bending. This tendency may be the same at a higher deformation rate. The specific impact energy also indicates that foams without PA can absorb a higher amount of energy as the crack does not propagate in the direction of the impact according to the video recording.

3.4 Post-impact residual strength test

The effect of impact on the residual strength was also investigated (see Table 3). After the impact of 1 J, the residual flexural strength of the foam-PA samples does not change. However, the scatter is much higher, indicating that due to the inhomogeneity of the material, in some cases the impact caused minor damage that led to the premature fracture during the post-impact test.

The AlSi12 foam's behavior is very different, the flexural strength of the AlSi12 foam is about the third after the impact of 1 J. This huge change can be attributed to the impact-initiated crack, which becomes visible on the recorded videos even at small loads. The different sample width may also affect the results. (The sample width was reduced from 20 mm to 10 mm to fit the impactor tester.) Further investigations are needed to confirm the role of sample's geometry on post-impact flexural strength.

4 Conclusion

The hot-pressing method was applied to produce layered structured AlSi12 foam–polyamide 6 composites with different PA content and porosities. The layered structure was produced by hot-pressing polyamide 6 (PA) sheets with thicknesses of 1 mm, 3 mm and 5 mm into the pores of an open-cell AlSi12 metal foam on both sides (PA_1, PA_ and PA_5). The following conclusions can be drawn from the three-point bending, Charpy impact and post-impact test results:

- The structural investigation revealed that the infiltration depth should be at least the pore size of the foam to avoid voids at the metal-PA interface and to have a satisfactory infiltration.
- The flexural strength and the absorbed impact energy of the metal foam-PA composite increased with increasing PA content. And PA_3 showed the highest specific flexural strength, which was about 10% higher than the specific flexural strength of the AlSi12 foam.
- The PA_5 had the highest Charpy impact strength which was 50.8 ± 10.3 kJ/m^2, twice as much the impact strength of PA_1.
- The post-impact test revealed that while the 1 J impact affected the residual strength of the AlSi12 foam, the metal foam-PA samples' bending properties did not change due to the 1 J impact.

References

[1] Refiadi, G., Aisyah, I. S., Siregar, J. P. "Trends in lightweight automotive materials for improving fuel efficiency and reducing carbon emissions", Automotive Experiences, 2(3), pp. 78–90, 2019.
https://doi.org/10.31603/ae.v2i3.2984

[2] Zhang, W., Xu, J. "Advanced lightweight materials for Automobiles: A review", Materials & Design, 221, 110994, 2022.
https://doi.org/10.1016/j.matdes.2022.110994

[3] Shipsha, A., Zenkert, D. "Compression-after-impact strength of sandwich panels with core crushing damage", Applied Composite Materials, 12, pp. 149–164, 2005.
https://doi.org/10.1007/s10443-005-1119-1

[4] Gustin, J., Joneson, A., Mahinfalah, M., Stone, J. "Low velocity impact of combination Kevlar/carbon fiber sandwich composites", Composite Structures, 69(4), pp. 396–406, 2005.
https://doi.org/10.1016/j.compstruct.2004.07.020

[5] Mannov, E., Schmutzler, H., Chandrasekaran, S., Viets, C., Buschhorn, S., Tölle, F., Mülhaupt, R., Schulte, K. "Improvement of compressive strength after impact in fibre reinforced polymer composites by matrix modification with thermally reduced graphene oxide", Composites Science and Technology, 87, pp. 36–41, 2013.
https://doi.org/10.1016/j.compscitech.2013.07.019

[6] Khaire, N., Gupta, M., Tiwari, G. "Blast resistance of graded aluminium foam core sandwich structure against blast loading", Materials Today: Proceedings, 87, pp. 159–163, 2023.
https://doi.org/10.1016/j.matpr.2023.03.220

[7] Guo, H., Zhang, J. "Expansion of sandwich tubes with metal foam core under axial compression", Journal of Applied Mechanics, 90(5), 051008, 2023.
https://doi.org/10.1115/1.4056686

[8] Omar, M. Y., Xiang, C., Gupta, N., Strbik III, O. M., Cho, K. "Syntactic foam core metal matrix sandwich composite under bending conditions", Materials & Design, 86, pp. 536–544, 2015.
https://doi.org/10.1016/j.matdes.2015.07.127

[9] Kemény, A., Pados, G., Károly, D., Orbulov, I. N. "The effects of various adhesives on multiple types of quasi-static mechanical properties of rectangular and square aluminum hollow sections filled with composite metal foam cores", Advanced Engineering Materials, 26(9), 2302066, 2024.
https://doi.org/10.1002/adem.202302066

[10] Huang, P., Sun, X., Su, X., Gao, Q., Feng, Z., Zu, G. "Three-point bending behavior of aluminum foam sandwich with different interface bonding methods", Materials, 15(19), 6931, 2022.
https://doi.org/10.3390/ma15196931

[11] Khalili, S., Khalili, S. M. R., Farsani, R. E., Mahajan, P. "Flexural properties of sandwich composite panels with glass laminate aluminum reinforced epoxy facesheets strengthened by SMA wires", Polymer Testing, 89, 106641, 2020.
https://doi.org/10.1016/j.polymertesting.2020.106641

[12] Al-Khazraji, M. S., Bakhy, S. H., Jweeg, M. J. "Composite sandwich structures: review of manufacturing techniques", Journal of Engineering, Design and Technology, 22(5), pp. 1616–1636, 2024.
https://doi.org/10.1108/JEDT-03-2022-0141

[13] Yazdani Sarvestani, H., Akbarzadeh, A. H., Niknam, H., Hermenean, K. "3D printed architected polymeric sandwich panels: Energy absorption and structural performance", Composite Structures, 200, pp. 886–909, 2018.
https://doi.org/10.1016/j.compstruct.2018.04.002

[14] Tarlochan, F. "Sandwich structures for energy absorption applications: A review", Materials, 14(16), 4731, 2021.
https://doi.org/10.3390/ma14164731

[15] Pozorska, J., Pozorski, Z. "Analysis of the failure mechanism of the sandwich panel at the supports", Procedia Engineering, 177, pp. 168–174, 2017.
https://doi.org/10.1016/j.proeng.2017.02.213

[16] Kotzem, D., Tazerout, D., Arold, T., Niendorf, T., Walther, F. "Failure mode map for E-PBF manufactured Ti6Al4V sandwich panels", Engineering Failure Analysis, 121, 105159, 2021.
https://doi.org/10.1016/j.engfailanal.2020.105159

[17] Yan, B., Wang, X., Pan, S., Tong, M., Yu, J., Liu, F. "Stability and failure of the edge-closed honeycomb sandwich panels with face/core debonding", Applied Sciences, 10(21), 7457, 2020.
https://doi.org/10.3390/app10217457

[18] Chen, J. "Predicting progressive delamination of stiffened fibre-composite panel and repaired sandwich panel by decohesion models", Journal of Thermoplastic Composite Materials, 15(5), pp. 429–442, 2002.
https://doi.org/10.1177/0892705702015005736

[19] Schubel, P. M., Luo, J.-J., Daniel, I. M. "Impact and post impact behavior of composite sandwich panels", Composites Part A: Applied Science and Manufacturing, 38(3), pp. 1051–1057, 2007.
https://doi.org/10.1016/j.compositesa.2006.06.022

[20] Collins, T. J. "ImageJ for microscopy", BioTechniques, 43(sup1), pp. S25–S30, 2007.
https://doi.org/10.2144/000112517

[21] Kostopoulos, V., Baltopoulos, A., Karapappas, P., Vavouliotis, A., Paipetis, A. "Impact and after-impact properties of carbon fibre reinforced composites enhanced with multi-wall carbon nanotubes", Composites Science and Technology, 70(4), pp. 553–563, 2010.
https://doi.org/10.1016/j.compscitech.2009.11.023

[22] MSZT "MSZ EN ISO 7438:2021 Metallic materials. Bend test (ISO 7438:2020)", Hungarian Standards Institution, Budapest, Hungary, 2021.

[23] Gibson, L. J. "Mechanical behavior of metallic foams", Annual Review of Materials Science, 30, pp. 191–227, 2000.
https://doi.org/10.1146/annurev.matsci.30.1.191

[24] Olurin, O. B., McCullough, K. Y. G., Fleck, N. A., Ashby, M. F. "Fatigue crack propagation in aluminium alloy foams", International Journal of Fatigue, 23(5), pp. 375–382, 2001.
https://doi.org/10.1016/S0142-1123(01)00010-X

[25] Lázaro, J., Solórzano, E., Rodríguez Pérez, M. A., García-Moreno, F. "Pore connectivity of aluminium foams: effect of production parameters", Journal of Materials Science, 50(8), pp. 3149–3163, 2015.
https://doi.org/10.1007/s10853-015-8876-5